Research paper

Expression mapping of GREM1 and functional contribution of its secreting cells in the brain using transgenic mouse models

Peijia Yao [a,1], Xueli Liu [a,b,1], Qiang Miao [a,1], Changxue Li [a], Huaixiang Zhou [a], Huiliang Li [c,d], Xinliang Mao [e,**], Xiaoyi Fang [b,**], Ningning Li [a,d,*]

[a] Tomas Lindahl Nobel Laureate Laboratory, The Seventh Affiliated Hospital, Sun Yat-Sen University, Shenzhen 518107, China
[b] Department of Neonatology, The Seventh Affiliated Hospital, Sun Yat-sen University, Shenzhen 518107, China
[c] Wolfson Institute for Biomedical Research, Division of Medicine, Faculty of Medical Sciences, University College London, United Kingdom
[d] China-UK Institute for Frontier Science, Shenzhen 518107, China
[e] Perfect Life and Health Institute, Zhongshan, 528454, Guangdong, China

A B S T R A C T

GREMLIN1 (GREM1) is a secreted protein that antagonizes bone morphogenetic proteins (BMPs). While abnormal GREM1 expression has been reported to cause behavioral defects in postpartum mice, the spatial and cellular distribution of GREM1 in the brain and the influence of the GREM1-secreting cells on brain function and behavior remain unclear. To address this, we designed a genetic cassette incorporating a 3×Flag-TeV-HA-T2A-tdTomato sequence, resulting in the creation of a novel Grem1Tag mouse model, expressing an epitope tag (3×Flag-TeV-HA-T2A) followed by a fluorescent reporter (tdTomato) under the control of the endogenous Grem1 promoter. This design facilitated precise tracking of the cell origin and distribution of GREM1 in the brain using tdTomato and Flag (or HA) markers, respectively. We confirmed that the Grem1Tag mouse exhibited normal motor, cognitive, and social behaviors at postnatal 60 days (P60), compared with C57BL/6J controls. Through immunofluorescence staining, we comprehensively mapped the distribution of GREM1-secreting cells across the central nervous system. Pervasive GREM1 expression was observed in the cerebral cortex (Cx), medulla, pons, and cerebellum, with the highest levels in the Cx region. Notably, within the Cx, GREM1 was predominantly secreted by excitatory neurons, particularly those expressing calcium/calmodulin-dependent protein kinase II alpha (Camk2a), while inhibitory neurons (parvalbumin-positive, PV$^+$) and glial cells (oligodendrocytes, astrocytes, and microglia) showed little or no GREM1 expression. To delineate the functional significance of GREM1-secreting cells, a selective ablation at P42 using a diphtheria toxin A (DTA) system resulted in increased anxiety-like behavior and impaired memory in mice. Altogether, our study harnessing the Grem1Tag mouse model reveals the spatial and cellular localization of GREM1 in the mouse brain, shedding light on the involvement of GREM1-secreting cells in modulating brain function and behavior. Our Grem1Tag mouse serves as a valuable tool for further exploring the precise role of GREM1 in brain development and disease.

1. Introduction

Bone morphogenetic proteins (BMPs) are a group of potent morphogens that are critical for the development and function of the central nervous system (Hart and Karimi-Abdolrezaee, 2020). The human genome contains >20 types of heterodimers or homodimer BMPs. According to the sequence homology of their amino acids, structures, and functions, they are divided into four separate subfamilies: (1) BMP2 and 4; (2) BMP5, 6, 7, 8a, and 8b; (3) BMP9 and 10; and (4) BMP12, 13, 14 (Bal et al., 2020). The BMPs exert their cellular response through two types of receptors: type I (BMPR1a, BMPR1b, ACVR1 and ACVR1b) and type II (BMPR2, ACVR2a, and ACVR2b), both of which are serine/threonine protein kinases (David and Massague, 2018). During the developmental stage, although widely expressed in telencephalon, BMP ligands (BMP2/4/5/6/7) limit the growth of the neuroectoderm by inhibiting cell proliferation and inducing local cell death (Furuta et al.,

1997). BMP receptors are also extensively expressed in the CNS (Central Nervous System), especially during development, followed by restricted distribution of BMPR2 in the cortex and hippocampus as well as ACVR2a/2b in the dentate gyrus in adulthood (Söderström et al., 1996). Meanwhile, BMP signaling is essential for homeostatic functions in the CNS. There is growing evidence that BMP signaling regulates CNS injury/repair, such as ischemic brain injury, frontotemporal dementia, spinal cord injury and demyelinating conditions (Ding et al., 2022; Petersen et al., 2021; Pous et al., 2020; Setoguchi et al., 2004). Additionally, BMP plays an essential role in maintaining homeostatic functions in various tissue types of adult vertebrates, especially in the context of brain tumors (Sun et al., 2022). Beyond these aspects, the bioavailability of BMPs is regulated by diffusible BMP antagonists, such as Noggin, Chordin, and GREM1. These antagonists have been demonstrated to inhibit BMPs action across different cell types and developmental stage-specific contexts, providing precise spatiotemporal regulation of the pathway (Correns et al., 2021). For instance, the roles of noggin and chordin have been partially elucidated, as they are required for forebrain development (Bachiller et al., 2000).

Recently, GREMLIN1 (GREM1) has attracted more attention because of its various biological functions. It is a secreted glycoprotein formed by 184 amino acids and shares a conserved cysteine-rich region containing a cysteine knot motif, belonging to the transforming growth factor-β (TGF-β) superfamily (Marquez-Exposito et al., 2020). Studies have reported that GREM1 can restrict BMP activity by antagonizing BMP2/4/7 from binding to their receptors, subsequently inhibiting the transduction of Smad signals. This positions GREM1 as an antagonist of BMPs (Church et al., 2015). Additionally, GREM1 showed the capacity to bind and activate vascular endothelial growth factor receptor 2 (VEGFR2), and the interaction between them is independent of BMPs (Mitola et al., 2010). Not only is GREM1 structurally similar to vascular endothelial growth factor A (VEGF-A), a well-known cystine node homologous secreted ligand for VEGFR2, but both exhibit high affinity for VEGFR2, with 47 nM and 3 nM, respectively, (Claesson-Welsh, 2010; Maiolo et al., 2012). In homeostasis, GREM1 depletion leads to haematopoietic failure and disturbs normal bowel epithelial function in adult by tamoxifen administration using a ubiquitous Cre recombinase in ROSA26-CreER[T2]: Grem1 flox/flox mice (Rowan et al., 2020). In addition, GREM1 causes a transient increase in bone formation and bone mass regulation due to BMP signaling activity from conditional deletion of *Grem1* in the bone at one month (Gazzerro et al., 2007). GREM1 secreted from PDGFRA^{low} cells and CD81^{+} cells also plays a critical role in maintaining robust intestinal stem cell viability (Kraiczy et al., 2023). Although the role of GREM1 has been well studied in maintaining intestinal stem cells and their niche, and in regulating bone formation in homeostatic conditions, the research investigating the biological implications of GREM1 under physiological and pathological conditions of the brain is still insufficient.

Up to date, accumulating evidence suggests that GREM1 may be a critical regulator in the CNS. A conceivable genetical association has been established between *Grem1* and neuropsychiatric disorders because the *Grem1*-encoding gene is located in the 15q13.3 chromosomal region (Topol et al., 2000). Notably, both microduplication and deletion at 15q13.3 contribute to severe clinical phenotypes, including autism spectrum disorder (ASD), mood disorders, seizures, and attention-deficit/hyperactivity disorder (ADHD), with different degrees of penetrance and severity (Antony et al., 2023). Early studies have also shown a high expression of *GREM1* in the human brain (Topol et al., 2000). Recently, conditional knockout of *Grem1* from the dorsal terminal brain of mice could lead to a reduction of thickness of the forebrain and midbrain, and impair the movement balance in mice, indicating that GREM1 is required for the development of the brain (Ichinose et al., 2021). Besides, GREM1 may be a potential agent for neuron degeneration disorders such as Parkinson's Disease and ischemic stroke. Treatment with GREM1 protected dopamine neurons against neurotoxin MPP[+]/MPTP-induced cell death (Phani et al., 2013). The expression of GREM1 in the serum of ischemic stroke patients had a marked decrease, but increased significantly after treatment, suggesting GREM1 may play a role in regulating neuroinflammation and nerve recovery after stroke (Fan et al., 2020). However, the specific localization of GREM1 expression and the function of GREM1-secreting cells in the brain have not yet been clarified.

In the present study, we focus on the expression of the BMP antagonist GREM1, as well as the effects of GREM1-secreting-cell depletion in the mouse brain. We first assessed the source of GREM1 in mouse brain using the Grem1-3×Flag-TeV-HA-T2A-tdTomato transgenic reporter mouse. Next, by tamoxifen-induced DTA in the *Grem1*-CreER[T2] : DTA mice, we eliminated a subset of GREM1-secreting-cells in mice to examine their functional contribution in the brain.

2. Materials and methods

2.1. Construction of Grem1-3×Flag-TeV-HA-T2A-tdTomato mouse

Mice were housed in specific pathogen-free (SPF) facilities in the Center of Laboratory Animal Science, Southern University of Science and Technology, China. Six mice per each cage were housed in transparent plastic cages with free access to water and food, and the temperature was controlled at $23 \pm 1\ ^\circ$C with relatively stable humidity (50 $\pm$ 10%) and a light/dark cycle of 12/12 h (lights on at 7:00). All experiments were performed by the National Institutes of Health Guide for the Care and Use of Laboratory Animals (NIH Publication No. 80–23, revised 1996), and the experimental procedures were approved by the Animal Care Committee of the Southern University of Science and Technology, China.

Under the conditions of CRISPR-Cas9 gene editing technology, we inserted the exogenous sequence of 3×Flag-TeV-HA-T2A-tdTomato behind the second exon of the *Grem1* gene in C57BL/6J mouse embryonic cells, thereby constructing a mouse strain containing the Grem1-3×Flag-TeV-HA-T2A-tdTomato allele (Grem1Tag mice). Grem1Tag transgenic mice were genotyped using WT allele and mutant allele primer pairs with polymerase chain reaction (PCR). A 538 base pair (bp) band corresponded to the wild-type (WT) allele, while a 408 bp band indicated the presence of the mutant allele. Heterozygotes exhibited both bands. Homozygous WT mice displayed a single band at 538 bp, while homozygous mutants showed a single band at 408 bp.

WT allele Forward primer: 5'-CAACAGCCGCACTATCATCAAC-3'.
WT allele Reverse primer: 5'-CACAATGACAAAGCCAACTACAGC-3'.
mutant allele Forward primer: 5'-TATGGCCAGTGCAACTCCTTCTA-3'.
mutant allele Reverse primer: 5'-CTCTTTGATGACCTCCTCGCC-3'.

2.2. Grem1-CreER[T2] : DTA mouse

Grem1-CreER[T2] and Rosa26-loxP-stop-loxP-DTA mice were purchased from Cyagen (Suzhou, China). Then *Grem1*-CreER[T2] : DTA mice were generated by crossing the *Grem1*-CreER[T2] and Rosa26-loxP-stop-loxP-DTA mice. For adult induction, tamoxifen suspended in corn oil (100 mg/kg) was administered once daily via oral gavage to mice aged between postnatal days 42 and 49 (P42 to P49).

2.3. Open field test (OFT)

An Open Field Test (OFT) paradigm was employed to assess rodent locomotor activity and anxiety phenotypes. Mice were allowed a 30 min acclimation period before the test. The experiment utilized an open field box measuring 40 cm in length, 40 cm in width, and 40 cm in height. The field was divided into 16 squares, with the central 4 squares designated as the center area (20 cm × 20 cm). During the 10 min formal test, mice were placed in the open field and observed. The SMART 3.0 system (Panlab, Spain) was used to record the distance traveled and time spent in each zone (Chang et al., 2023).

2.4. Elevated plus maze (EPM) test

The elevated plus maze (EPM) is a classic behavioral test to study anxiety-like behaviors in rodents. The apparatus elevated 50 cm above the ground consisting of four arms arranged in the shape of a plus sign. Two opposing open arms (5 cm × 35 cm) and two closed arms (5 cm × 35 cm) with 15 cm high walls of the same dimensions are crossed vertically to each other at the central platform. The mice were individually located in the center of the maze facing an open arm and allowed 10 min of free exploration. Entry was recognized as all four paws in the arms. Exploration time of the mice in the two types of arms and total traveled distance were recorded. Then, the total movement distance and the time spent in each area were recorded and analyzed using SMART 3.0.

2.5. Novel object recognition test (NOR)

The novel object recognition (NOR) test is based on the rationale that mice tend to explore new objects more than familiar ones. We therefore used NOR to assess whether transgenic cassette (3×Flag-TeV-HA-T2A-tdTomato) impairs cognition in Grem1Tag mice. NOR was divided into two main phases: familiarization and recognition test phases. Mice were given 30 min for environmental adaptation before the start of NOR. (1) In the familiarization phase, mice were allowed to explore an open field (40 cm long × 40 cm wide × 45 cm high) freely for 10 min where two same objects 1 and 2 were placed at marked points with 10 cm. The mice were then taken back in the home cage and rested for one hour. (2) In the recognition test phases, the mice were re-exposed to the open field where object 2 was replaced with the new object. The time of exploration of objects 1 and 2, as well as object 1 and the new object, was recorded and analyzed by SMART 3.0.

2.6. Three-chamber social interaction test (TCT)

The social preference and social novelty of mice were examined by a three-chamber social interaction test. An open rectangular box (60 cm long × 40 cm wide × 25 cm high) with two medical-organic baffles in the middle is divided into three separate chambers, each with a small door below the baffle that can be opened and closed to allow the mouse free access to each chamber. The corners of the left and right chambers had a plastic grid restraint. The experiment was divided into 3 stages: (1) Habituation: the mice were placed in the central chamber, and the doors of the left and right baffles were opened to allow them to explore freely for 10 min to get familiar with the environment; (2) Sociability: after 10 min, the mice were put back into the central chamber, the doors of the left and right baffles were closed and a mouse with same gender and age was placed in the restraints of the left chamber (stranger1), while another was kept vacant (empty). The small doors of the left and right baffles were opened to allow free movement for 10 min and the activities recorded; (3) Social novelty: After the sociability phase, the mice were put back into the central chamber, the small doors of the left and right baffles were closed. Stranger 1 continued to be kept in restraint of the left chamber, then another mouse with same gender and age (stranger 2) was put into the restraint of the right chamber, the small doors of the left and right baffles were opened to allow mice to explore freely for 10 min. At the end of the experiment, the mice were put back into the rearing cage, the behavior box was cleaned, and the exploration time of stranger 1, stranger 2, and the empty chamber by the experimental mice at each phase was recorded. During the experiment, the light inside the behavior box was maintained at 40 lx, and the temperature was kept at 24 °C. The experimenter, avoided being in the sight of the mice, reduced the noise generation, and maintained the ambient volume below 30 dB to keep quiet. The interaction time of mice with stranger 1 or 2 was recorded and analyzed by SMART 3.0.

2.7. Immunofluorescence staining

After behavioral tests, mice were anesthetized with Avertin and then sequentially perfused with cold PBS and 4% PFA via the heart. Subsequently, the brains were dehydrated with 10%, 20% and 30% gradient sucrose solution for 24 h, respectively. After embedding with Tissue-Tek OCT (Sakura Seiki, Japan), brain sagittal sections (30 μm) and coronal sections (10 μm) were cut using a cryostat microtome (Leica CM1850, Germany). Subsequently, brain slices were first rinsed with 1×PBS three times (10 min/session) and then blocked with blocking solution (5% BSA supplemented with 0.3% Triton X-100 in PBS) for 1 h at room temperature, followed by incubation with primary antibodies at 4 °C overnight. The next day, brain slices were rinsed three times with 1×PBS, and then incubated with the corresponding fluorescent secondary antibodies for 90 min. After washing three times with 1×PBS, the slices were treated with 1 μg/mL DAPI for 10 min at room temperature. The following commercially available antibodies were used: rabbit monoclonal anti-Neun (Abcam, ab177487), guinea pig polyclonal anti-Neun (Oasis Biofarm, OB-PGP006), mouse monoclonal anti-Flag (CST, 8146), rabbit monoclonal anti-Flag (CST, 14793), rabbit monoclonal anti-HA (CST, 3724), chicken polyclonal anti-mCherry (Abcam, ab205402), rabbit monoclonal anti-Iba-1 (FUJIFILM, 018–28523), goat monoclonal anti-GFAP (Abcam, ab302644), rabbit monoclonal anti-Olig2 (Abcam, ab109186), mouse monoclonal anti-MOG (Millipore, MAB5680), guinea pig polyclonal anti-PV (Oasis Biofarm, OB-PGP005), mouse monoclonal anti-Camk2a (Santa Cuz, sc-5306). Fluorescent images were captured through fluorescence microscope (ZEISS Axio Imager 2, Germany) and confocal microscope (ZEISS LSM980, Germany). Analysis and quantification were performed by ImageJ software.

2.8. Flag and tdTomato signal quantification in sagittal brain regions of Grem1Tag mice

For localization and quantification of Flag and tdTomato signals in the sagittal brain region of Grem1Tag mice, images were captured using a ZEISS Axio Imager 2 microscope at a 20× objective lens. The ZEISS software ZEN blue was used to stitch the captured images into a complete sagittal image of the whole brain. Afterward, 2D Flag and tdTomato signals was rendered by IMARIS "Spots" function with same parameters respectively. Brain region partitions were adapted from Paxinos and Franklin's mouse brain in stereotaxic coordinates whilst the IMARIS MATLAB-based (MathWorks) plugin "close to Surface Objects" was utilized to assess the number of Flag and tdTomato signals puncta with 0 distance of the surface. The IMARIS surface function was used to calculate area of each brain region. Lastly, the collected value percentages of Flag and tdTomato signals in each brain region as well as the intensity were calculated.

2.9. Three-dimensional (3D) reconstruction for signal quantification

The 30 μm coronal slices were subjected to overnight staining using anti-Iba-1, anti-Neun, and anti-mCherry antibodies. Subsequently, secondary antibody staining was carried out using Alexa Fluor 488 for Iba-1 and Neun, and Alexa Fluor 568 for mCherry. Imaging was conducted on a Zeiss LSM980 microscope with a 100× /1.3 NA oil objective. The imaging parameters, including laser power, gain, and offset, were kept consistent throughout all experiments. The number of tdTomato signals reconstructed using the IMARIS "Spots" function was quantified via IMARIS software to create a 3D surface rendering of the microglia and neuron cells which contained tdToamto signals, with a same threshold established to ensure accurate reconstruction of microglial and neuron cell bodies.

2.10. Statistical analysis

Independent sample *t*-tests were applied to assess the difference in
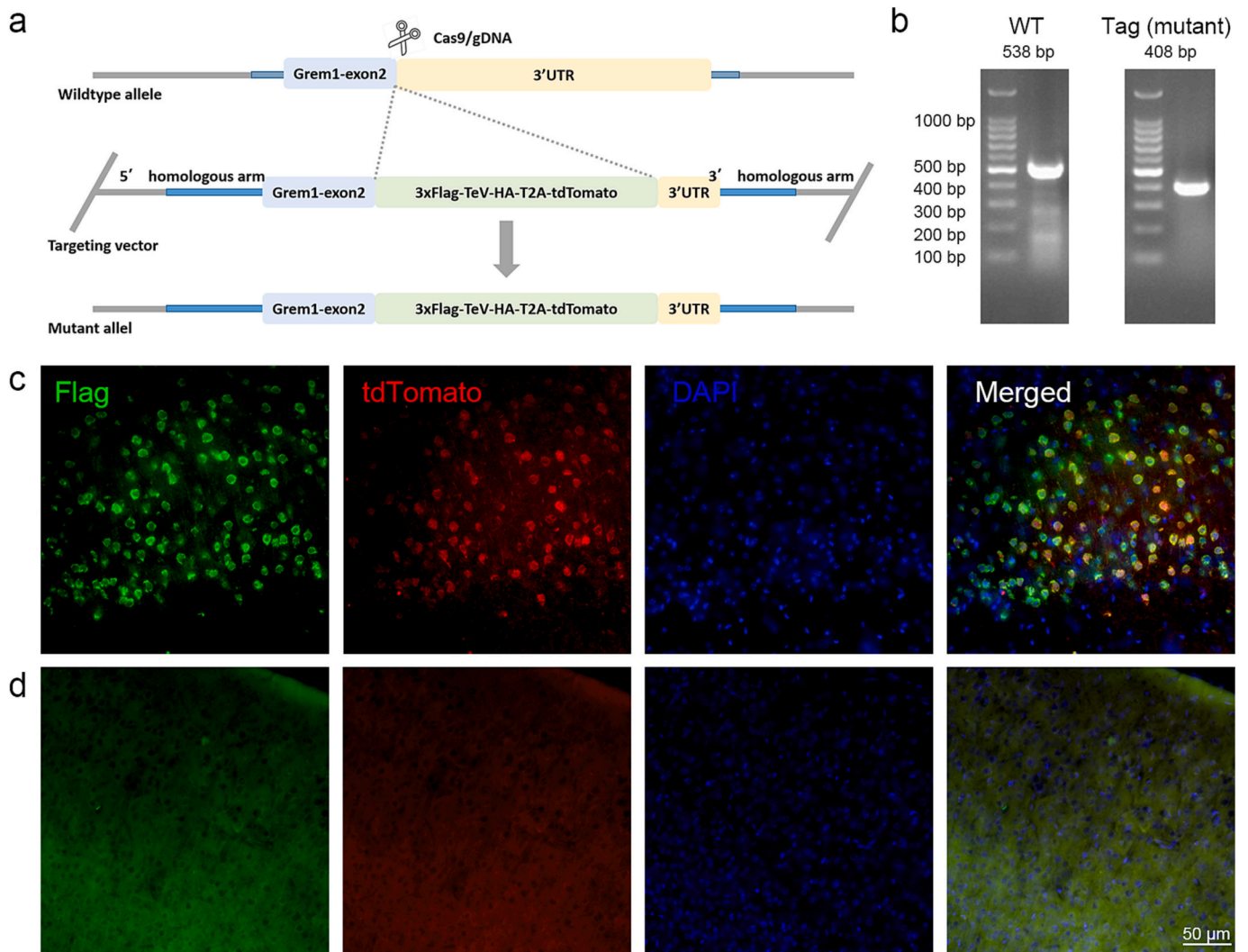
Fig. 1. Generation of a Grem1Tag mouse.
(a) Schematic representation of the strategy for the construction of Grem1Tag mouse. (b) PCR genotyping analysis showing a heterozygous Grem1Tag mouse with a wild-type (WT) allele (538 bp band) and a mutant allele (408 bp band). (c) Immunofluorescence (IF) staining showing GREM1 molecules labeled by Flag (Green) and cells expressing GREM1 marked by tdToamto (Red), in the cerebral cortex of Grem1Tag mice. (d) IF staining on WT control tissue using the same primary antibodies and second antibodies as those used in (c). ZEISS Axio Imager 2 microscope using a 40× / 0.95 NA objective.
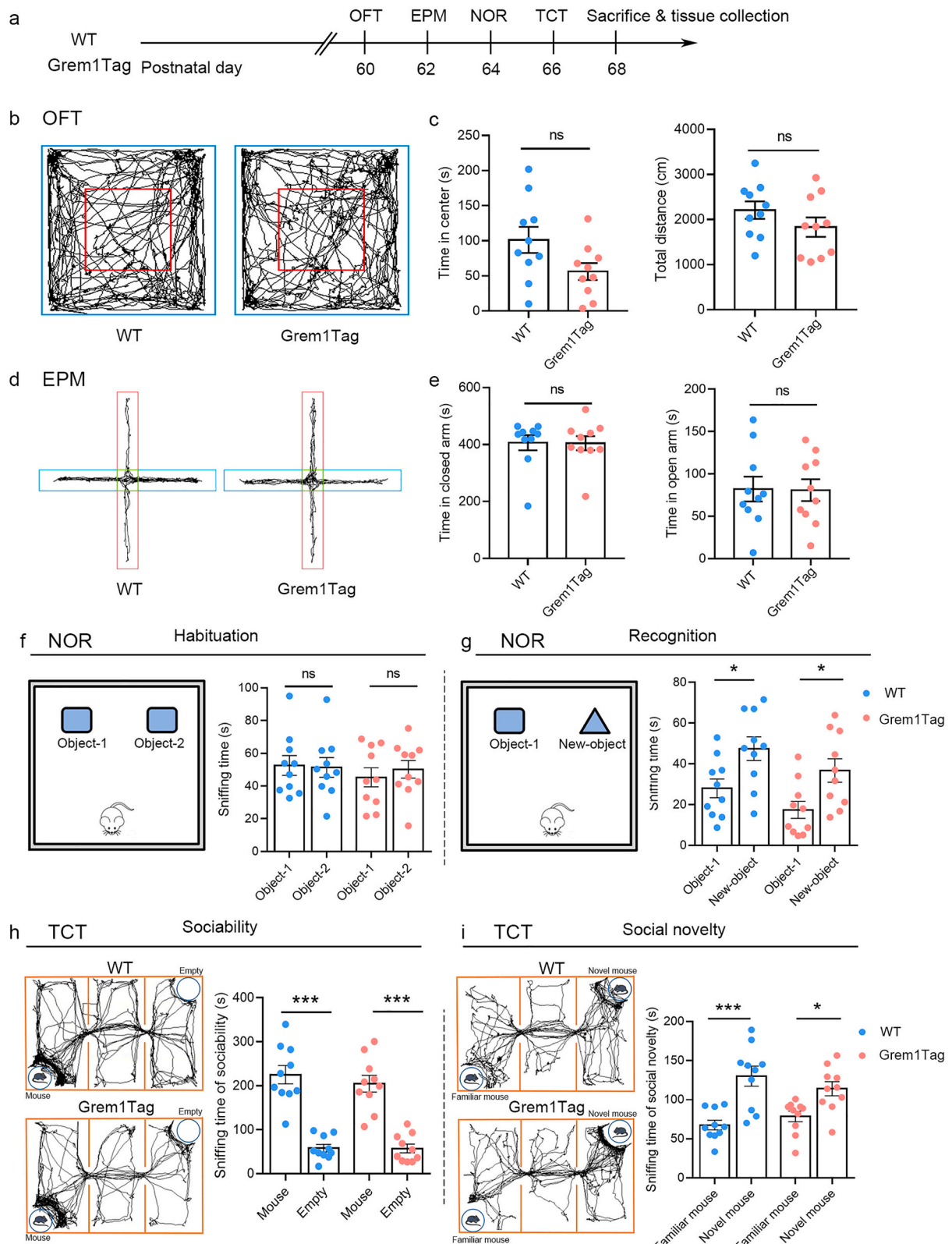
experimental data of the open field test, elevated plus maze, new object recognition test, three chamber socialization tests, etc. Assumptions of normality and homogeneity of variances were evaluated by Shapiro-Wilk tests and Levene's tests, respectively. The results in the graphs were expressed as mean ± standard error of the mean (SEM). A value of $p < 0.05$ was defined as statistically significant. GraphPad Prism 8.0 was used to synthesize graphics.

3. Results

3.1. Construction of Grem1Tag mouse

The *Grem1* gene (NCBI Reference Sequence: NM_011824.4) in mice is located on chromosome 2 and consists of two exons. In this study, to enable effective tracking of GREM1, we engineered a mouse containing a Grem1-3×flag-HA-TeV-T2A-tdTomato allele. The construction of this allele involved the use of CRISPR/Cas9 technology to remove the TAA terminator within the coding sequence (CDS) region of the exon2 of *Grem1*. Subsequently, we inserted the cassette '3×flag-HA-TeV-T2A-tdTomato', preserving the original 3' UTR of *Grem1* (Fig. 1a). The sequence of the cassette is provided in Supplementary Table. S1 and

includes several functional elements: epitope tags (3×Flag and HA) for GREM1 protein detection, a TeV protease recognition site for site-specific cleavage, a self-cleaving peptide (T2A) (Donnelly et al., 2001) and a tdTomato for localizing the GREM1-secreting cells. The targeting vector was microinjected into fertilized eggs of C57BL/6J strain mice using a microinjection technique with Cas9 mRNA and gRNA to obtain F0 generation Grem1Tag transgenic mice. Positive F0 mice were identified through PCR amplification and sequencing. These positive F0 mice were then mated with C57BL/6J mice to obtain positive F1 generation mice. Genotyping of the mice was performed using short fragment PCR, where a 538 bp band represented the wild-type (WT) allele, a 408 bp band indicated the presence of the mutant allele, and heterozygous individuals displayed both bands (Fig. 1b). Furthermore, immunofluorescence staining was conducted to confirm the successful transcription and translation of the inserted 3×Flag-TeV-HA-T2A-tdTomato tags. The presence of Flag and HA signals indicated the expression of GREM1 molecules, while the presence of the tdTomato signal indicated cells capable to secrete GREM1 (Fig. 1c and S1a). WT negative control corresponding to the primary antibody was used to demonstrate the specificity of the staining (Fig. 1d and S1b). The mice through these identification methods were classified as Grem1Tag transgenic-positive

a

WT
Grem1Tag   Postnatal day

OFT   EPM   NOR   TCT   Sacrifice & tissue collection

60   62   64   66   68

b   OFT

WT   Grem1Tag

c

d   EPM

WT   Grem1Tag

e

f   NOR   Habituation

g   NOR   Recognition

h   TCT   Sociability

i   TCT   Social novelty

(caption on next page)

Fig. 2. Behavioral assessments of Grem1Tag mice.

(a) Timeline of behavioral tests conducted on Grem1Tag mice versus wild-type (WT) mice. (b) Representative trajectory diagrams showing the time spent in each region of the open field box for both WT and Grem1Tag mice. Red boxes denote central area. (c) Bar chart illustrating the cumulative time spent in the central area (left panel) and the total distance traveled by Grem1Tag mice compared to WT mice (right panel) during a 10 min open field test (OFT). (d) Representative trajectory diagrams illustrating the exploration time of WT and Grem1Tag mice in both the open (denoted in blue) and closed (denoted in red) arms of the elevated-plus-maze (EPM) during testing. (e) Bar graphs showing the cumulative time spent in the open and closed arms of the EPM test for Grem1Tag mice compared to WT mice. (f,g) Two phases of the Novel Object Recognition (NOR) test, including the habituation (f) and recognition phase (g). Left panels depict pattern diagrams of the testing, and right panels show the corresponding statistical graphs. (h,i) Two phases of the Three-Chamber Test (TCT), including the sociability (h) and social novelty (i) phase. Representative trajectory diagrams (left panels) and corresponding statistical graphs (right panels) illustrate the socialization time of WT and Grem1Tag mice spent with stranger1 mouse versus the empty cage (h) or with the stranger1 (familiar) mouse versus the stranger2 (novel) mouse (i). For all tests (OFT, EPM, NOR, and TCT), $n = 10$, male, P60 for both WT and Grem1Tag mice. Data are presented as means $\pm$ SEM. Statistical significance is determined by a two-tailed student t-test, ns, $p > 0.05$; *$p < 0.05$; **$p < 0.01$; ***$p < 0.001$; ****$p < 0.0001$.

mice.

3.2. Grem1Tag mice did not exhibit abnormalities in behavioral tests

No significant behavioral abnormalities were observed in Grem1Tag mice under standard housing conditions. To further confirm this, we conducted behavioral tests on adult mice (Fig. 2a), including the open field test (OFT), elevated plus maze (EPM) test, novel object recognition (NOR) test, and three-chamber test (TCT). In the OFT (Fig. 2b), we found no significant differences between Grem1Tag and wild-type mice in terms of the cumulative duration spent in the central area and total distance traveled (Fig. 2c). These results indicated that Grem1Tag mice did not display altered locomotor activity or anxiety-like behavior compared to their wild-type counterparts, which was further supported by the EPM results (Fig. 2d-e). Furthermore, the NOR and TCT were conducted to assess cognitive ability, sociability, and social novelty. The NOR results showed that Grem1Tag mice exhibited a similar preference for exploring new objects compared to their wild-type counterparts (Fig. 2f and g). Additionally, in the sociability phase of the TCT, the cumulative sniffing time between the mouse-containing box and the empty box did not differ significantly between Grem1Tag and wild-type mice (Fig. 2h). Similarly, in the social novelty phase, the cumulative sniffing time for the familiar mouse and the novel mouse did not differ significantly between Grem1Tag and wild-type mice (Fig. 2i). Overall, these results demonstrated that Grem1Tag mice did not exhibit impairments in cognitive function, social and anxiety behavior, or locomotor ability compared to wild-type mice.

3.3. Distribution pattern of Flag-labeled and tdTomato-labeled signal in the brain

T2A is a highly efficient self-sheared protein, separating the translated Grem1-3×Flag-TeV-HA-T2A-tdTomato protein into tdTomato remaining in the cytosol and Grem1–3×Flag-TeV-HA excreted out of cytosol. Therefore, we illustrated the distribution of GREM1 original signals labeled by a tdTomato antibody and the expression of GREM1 labeled by a Flag antibody through immunofluorescence staining across various brain regions using a general fluorescence microscope (Objective lens 20×). The results demonstrated that GREM1 signals were widespread in the brain when matching the sagittal section of the brain atlas (1.20 mm lateral to the midline). Based on the expression pattern of GREM1, we divided the entire brain into 11 major brain regions and quantified all the Flag-positive signals, which represent the quantity of GREM1 molecules using Imaris software. The analysis of the GREM1 signal percentages in the sagittal section revealed that cortex (Cx), midbrain (MB), and medulla had higher proportions of GREM1 signals, accounting for 24.12%, 13.24%, and 12.13%, respectively (Fig. 3a). Furthermore, the intensities of GREM1 signals were also correspondingly higher in the Cx, MB, and medulla regions with insignificant differences in intensity (Fig. 3b). These findings suggested that GREM1 may play an important role in these brain regions, particularly in the cortex.

On the other hand, the expression of the GREM1-secreting signal

labeled with tdTomato was also observed in 11 brain regions, with the following percentages: Cx 14.64%, Cerebellum (Cb) 12.13%, and medulla 10.66% (Fig. 3c). These findings align with the In Situ Hybridization (ISH) results from Allen's brain dataset, which can be accessed at https://portal.brain-map.org/. Both tdTomato and *Grem1*-ISH experiments indicate a higher proportion of *Grem1* expression, primarily in gray matter regions such as the cortex, cerebellum, and medulla. In contrast, lower levels of *Grem1* expression were observed in white matter regions, such as the corpus callosum (Fig. 3c and e). Moreover, based on the statistical results from both tdTomato and *Grem1*-ISH, we observed that brain regions exhibiting robust *Grem1* expression intensity were predominantly localized in gray matter areas abundant with, including the cortex, cerebellum, medulla, and thalamus. (Fig. 3d and f).

3.4. Specific cell types expressing GREM1 in the cerebral cortex of Grem1Tag mice

To investigate GREM1 specific cell types expressing tdTomato and GREM1, we focused on the cortex, where GREM1 expression is particularly enriched. Although the intensity of GREM1 expression is also high in other brain regions such as the medulla and thalamus, the follow-up studies focusing on the behavioral effects of GREM1 on emotion, socialization, and memory are highly correlated with cortex. By fluorescence co-localization staining, we utilized seven specific markers, Neun for neurons, Camk2a for excitatory neurons, PV for interneurons, Iba-1 for microglia, GFAP for astrocytes, Olig2 and MOG for oligodendrocytes. These markers were co-stained alongside tdTomato labeled with mCherry and GREM1 labeled with Flag. We found that neurons (Fig. 4a) including excitatory neurons (Fig. 4c), and interneuron (Fig. 4d), and microglia (Fig. 4b and 5a) demonstrated observable tdTomato signals. Notably, neurons displayed a more robust and abundant tdTomato signal compared to microglia (Fig. 5a and b). Interestingly, GFAP and oligodendrocytes did not demonstrate overlapping or closely associated signals with the tdTomato and GREM1 (Fig. S2b and S2c-d). In summary, our findings elucidate the secretion of GREM1 by neurons and microglia with Neun$^+$ and microglia$^+$ accounting for 91.24% and 3.76% of tdTomato$^+$ cells, respectively (Fig. 4e). Within this context, Camk2a$^+$ cell proportion was much higher than PV$^+$ cell proportion in tdTomato$^+$ cells in the cerebral cortex of Grem1Tag mice (Fig. 4f). Furthermore, the absence of GREM1 expression in oligodendrocytes suggested that GREM1 may not play a role in myelin sheath growth and development. These comprehensive results contribute to our understanding of the crucial involvement of GREM1 in central nervous system development and maintenance, underscoring its significance in neuronal processes and highlighting potential avenues for further research.

3.5. Evaluation of GREM1 production capacity

Based on the staining results above, tdTomato-positive signals were observed in neurons and microglia, indicating the potential of these two types of cells secreting GREM1. To quantify the production capacity indicated by tdTomato signal expression, Imaris software was utilized to analyze tdTomato signals using consistent computational parameters for
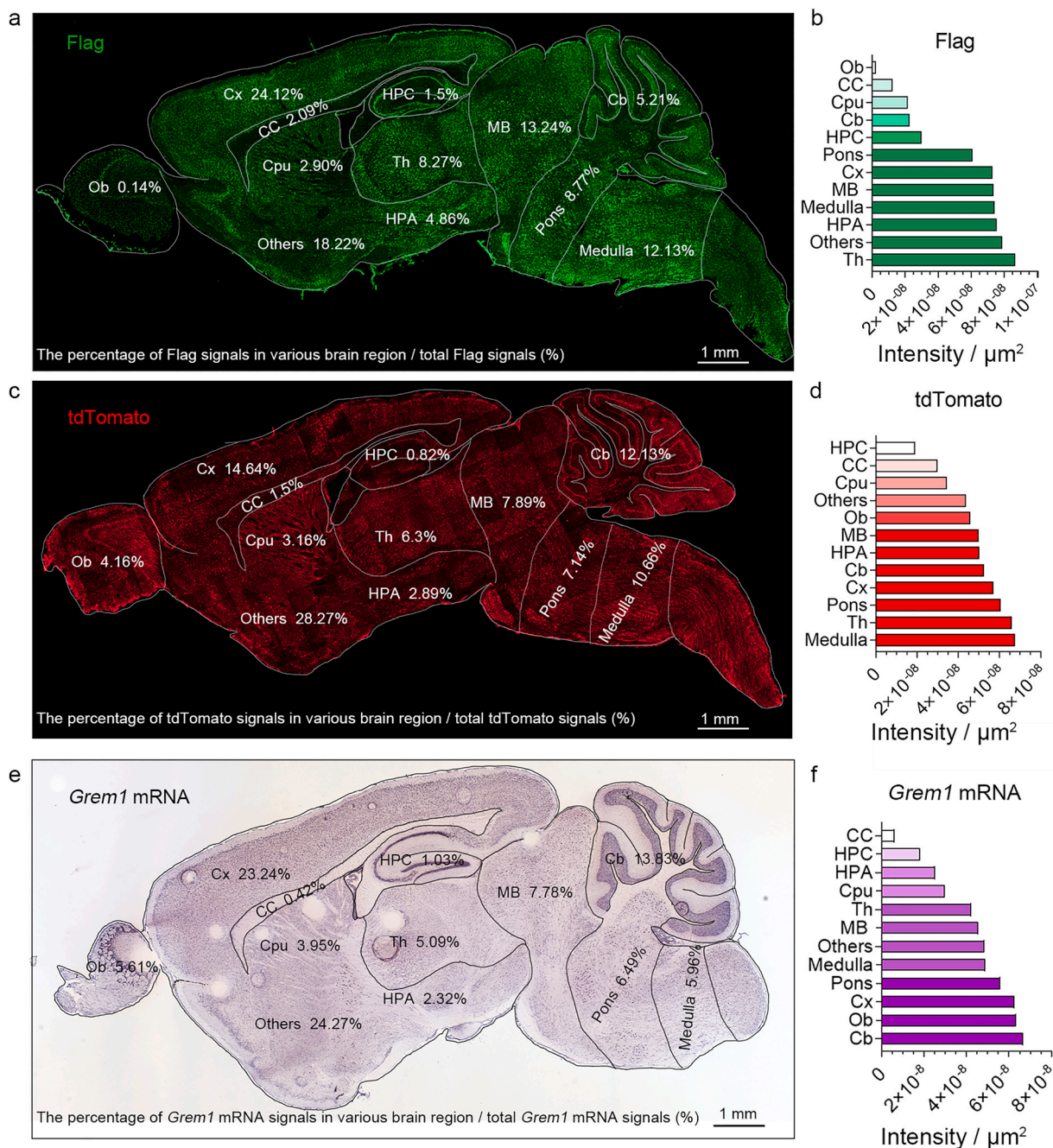
Fig. 3. Brain region distribution of GREM1 molecule and its secretion signal by Grem1Tag mice at P60.

(a) Brain atlas of mice with a sagittal section labeled by Flag antibody (1.20 mm lateral to the midline), adapted from Paxinos and Franklin's mouse brain in stereotaxic coordinates. The "others" refers to the proportion of GREM1-positive molecules in brain regions outside of the 11 major regions. (b) The signal intensity of the Flag in different brain regions. (c) Brain atlas of mice with a sagittal section labeled by mCherry antibody (1.20 mm lateral to the midline). (d) The signal intensity of the tdTomato in different brain regions. ZEISS Axio Imager 2 microscope using a 20× / 0.8 NA objective. (e) Brain atlas of mice with a sagittal section labeled by *Grem1* FISH probes. (f) The signal intensity of the *Grem1* mRNA in different brain regions.

Abbreviation: Ob: olfactory bulb, Cx: cerebral cortex, CC: corpus callosum, HPC: hippocampus, Cpu: corpus striatum, TH: thalamus, HPA: hypothalamus, MB: midbrain, Cb: cerebellum, Pons, Medulla, Others: Other than 11 brain regions.

each 3D cell. Our statistical analysis of the staining results demonstrated that neurons exhibited the highest production capacity for tdTomato, displaying approximately a 3-fold higher secretion capacity compared to microglia (Fig. 5a-c; The number of microglia cells, $n = 17$; The number of neuron cells, $n = 21$).

3.6. Ablation of GREM1-secreting cells led to abnormal behavior and brain damage in mice

To confirm the functional contribution of GREM1-secreting cells in the brain, we generated *Grem1*-CreER^{T2} : DTA (DTA$^+$) mice and *Grem1*-CreER^{T2} littermates as controls. In these mice, Cre-mediated excision of a STOP signal leads to the expression of the Diphtheria toxin (DTA) and thus ablation of GREM1-secreting cells. We administered seven daily
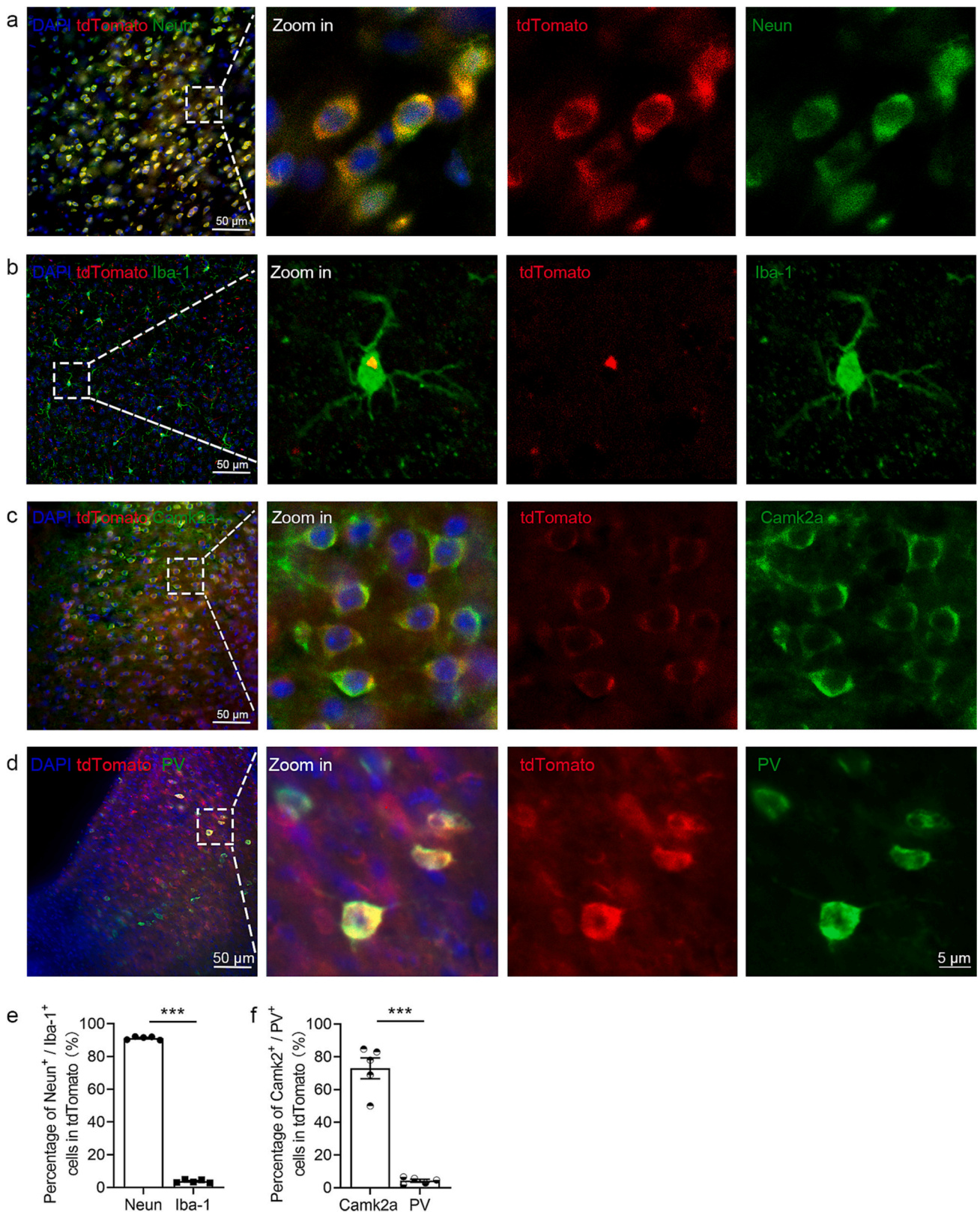
Fig. 4. Specific cell types expressing GREM1 in the cerebral cortex of Grem1Tag mice at P60.
Immunofluorescence staining with an anti-Neun, Iba-1, Camk2a, PV to label (a) neurons (b) microglia (c) excitatory neurons (d) interneurons (Green), and anti-mCherry antibody to label tdTomato (red). (e) Percentage of double positive cells (i.e., tdTomato$^+$ signals co-stained with Neun$^+$ or Iba-1$^+$ cells) in total tdTomato$^+$ cells in the cerebral cortex of Grem1Tag mice. (f) Percentage of double positive cells (i.e., tdTomato$^+$ neurons co-stained with Camk2a$^+$ or PV$^+$ neurons) in total tdTomato$^+$ neurons in the cerebral cortex of Grem1Tag mice. ZEISS Axio Imager 2 microscope using a 40× / 0.95 NA objective. (Neurons, $n = 5$ slices; iba1, $n = 5$ slices; Camk2a$^+$, $n = 6$ slices; PV$^+$, n = 5 slices, Grem1Tag male, P60). Data are presented as means ± SEM. Statistical significance is determined by a two-tailed student t-test, ns, no significant. $p > 0.05$; *$p < 0.05$; **$p < 0.01$; ***$p < 0.001$; ****$p < 0.0001$. The white arrow indicates the positive cells in the co-staining.
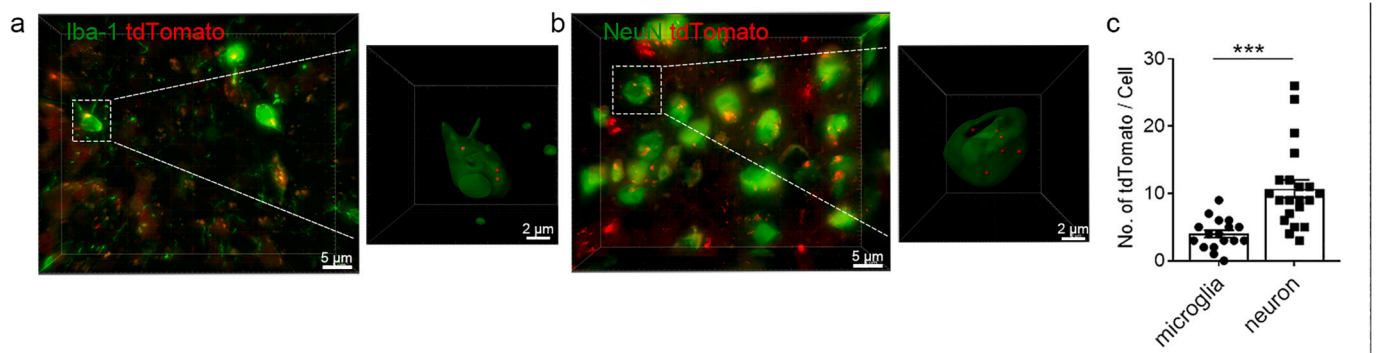
Fig. 5. Quantification of tdTomato signals and in the cerebral cortex of Grem1Tag mice at P60.
(a,b) 3D fluorescence reconstruction for co-staining of tdTomato (Red) with Iba-1 (a) and Neun (b) (Green). Zeiss LSM980 microscope using a 100× / 1.3 NA oil objective. (c) Quantification of secretory capacity in GREM1-secreting cells. The number of tdTomato signals within microglia cells and neurons was performed using Imaris software with consistent parameters (n = 17, microglia; n = 21, neuron from Grem1Tag male mice, $n = 3$, P60). Data are presented as means ± SEM. Statistical significance is determined by a two-tailed student *t*-test, ns, no significant. $p > 0.05$; *$p < 0.05$; **$p < 0.01$; ***$p < 0.001$; ****$p < 0.0001$.

doses of 2 mg subcutaneous tamoxifen starting at P42, followed by behavioral tests and measurement of mouse brain alterations at P56 (Fig. 6a). The OFT and EPM tests showed that DTA$^+$ mice exhibited shorter travel distances in the center area and open arms (Fig. 6b and c, respectively). In NOR tests, there was a significant decrease in exploration times toward novel context in DTA$^+$ mice versus the control mice (Fig. 6d). Meanwhile, we observed that DTA$^+$ mice exhibited an indistinguishable social interaction behavior toward a novel or familiar mouse in the TCT test (Fig. 6e). The above results displayed that ablation of GREM1-secreting cells resulted in anxiety behavior and memory impairment in mice. Furthermore, we observed pathological changes in the brain in DTA$^+$ mice. It was found that the number of Neun$^+$ GREM1$^+$ double positive cells decreased significantly in the cortical cortex (Fig. 6f and g). Similarly, the number of Iba-1$^+$ cells decreased significantly in the cortical cortex (Fig. S3a).

4. Discussion

The BMP signaling not only controls a variety of biological processes, including cell proliferation, differentiation, and apoptosis, but also is crucial in regulating the development and maintaining homeostasis of CNS (Bal et al., 2020; David and Massague, 2018; Furuta et al., 1997; Hart and Karimi-Abdolrezaee, 2020; Söderström et al., 1996). Furthermore, the BMP signaling pathway is modulated at the cellular or cytoplasmic level during neural induction (Manzari-Tavakoli et al., 2022). As an endogenous modulator of BMP signaling, *Grem1* marks committed layer V and VI glutamatergic neurons in the embryonic mouse brain and regulates early forebrain development and cortical formation (Ichinose et al., 2021). In terms of neurodevelopmental disorder, increased *Grem1* mRNA level was found in endothelial-specific 16p11.2 microdeletion mice, which develop autism spectrum disorder (ASD) symptoms that are characterized by diminished social interactions and communication, restricted and/or repetitive behaviors or interests, and abnormal sensory responses (Ouellette et al., 2020). Despite the above-mentioned research on developing brain, to date, no investigation has focused on the distribution pattern of GREM1 in the adult brain. Here, we successfully generated the Grem1Tag mice using CRISPR/Cas9 to insert the cassette '3×flag-HA-TeV-T2A-tdTomato' behind the exon2 of *Grem1* by which we could map out the distribution pattern of GREM1 and further determine where GREM1 originated from and where GREM1 was to go in cell levels at postnatal 60 days (Fig. S2a). The inclusion of the self-cleaving peptide T2A in Grem1Tag mice facilitated the seamless separation of the two proteins flanking the T2A sequence. Consequently, tdTomato signals served as a reliable indicator of GREM1 origin, while the presence of Flag or HA signals traced the expression of GREM1 protein. Our immunofluorescence staining results of Flag showed the

distribution map of GREM1 protein in mouse brains. Simultaneously, tdTomato revealed the full view of GREM1 origin, as tdTomato labeling correlates with *Grem1* mRNA expression levels. To further validate our research findings, we conducted statistical analysis and comparisons between our experimental data and the *Grem1* In Situ Hybridization (ISH) result from the Allen Brain Database. Although the comparative analysis revealed slight discrepancies in *Grem1* expression intensity in certain brain regions, the overall distribution pattern remained consistent, primarily concentrated in the gray matter areas such as the cortex and thalamus. These differences in *Grem1* expression intensity in specific brain regions may stem from variations in brain area delineation and differences in the shape of brain slices, leading to variations in surface area and consequently impacting signal intensity. Despite minor differences, our results demonstrate a substantial degree of consistency between the two statistical results, indicating a reliable depiction of *Grem1* distribution by Grem1Tag mice. At the cellular level, we observed a significantly higher abundance of Tdtomato signals in neurons compared to the relatively fewer signals in microglial cells. Upon performing 3D imaging and utilizing Imaris software for signal quantification, we determined that neurons exhibited approximately three times higher GREM1 secretion capability than microglial cells. Besides, distinct colocalization between Flag and Neun by immunofluorescence staining implied that effector cells of GREM1 were neurons. Notably, a previous report suggested that GREM1 typically acts on nearby or adjacent cells (Mitola et al., 2010; Worthley et al., 2015). In line with this, our data show that Flag staining exhibits a soma-like structure of cells that express tdTomato signals simultaneously (Fig. S2a). These results suggest that neurons may be enriched with relative receptors for GREM1 on the soma. In fact, there is a wide expression of BMP receptors in neurons, each exhibiting specific cell type expression patterns. For instance, in the development of the cortical cortex, the expression of BMPR1a/1b, ACVR2b, and ACVR1b/1/1c/2a, as well as BMPR2, correlated with the neurogenesis or differentiation of the upper-layer and deep-layer neurons based on the mouse scRNA-seq cortical neuron dataset (Ichinose et al., 2021; Yuzwa et al., 2017). This could explain why GREM1 expression (Flag staining) highlights the soma-like structure and is co-localized with neurons. However, there is a restricted distribution of BMPR2 in the cortex and hippocampus as well as ACVR2a/2b in the dentate gyrus in the hippocampus in adults (Söderström et al., 1996). To date, the exact BMP receptor corresponding to GREM1 still needs to be further elucidated.

Secreted proteins are an important category of drug targets for anticancer drug development. It seems that GREM1 can be defined as a potential anti-tumor target because accumulating evidence shows that Additionally, GREM1 promotes tumor growth. For example, GREM1 overexpression drives prostate cancer survival and proliferation through
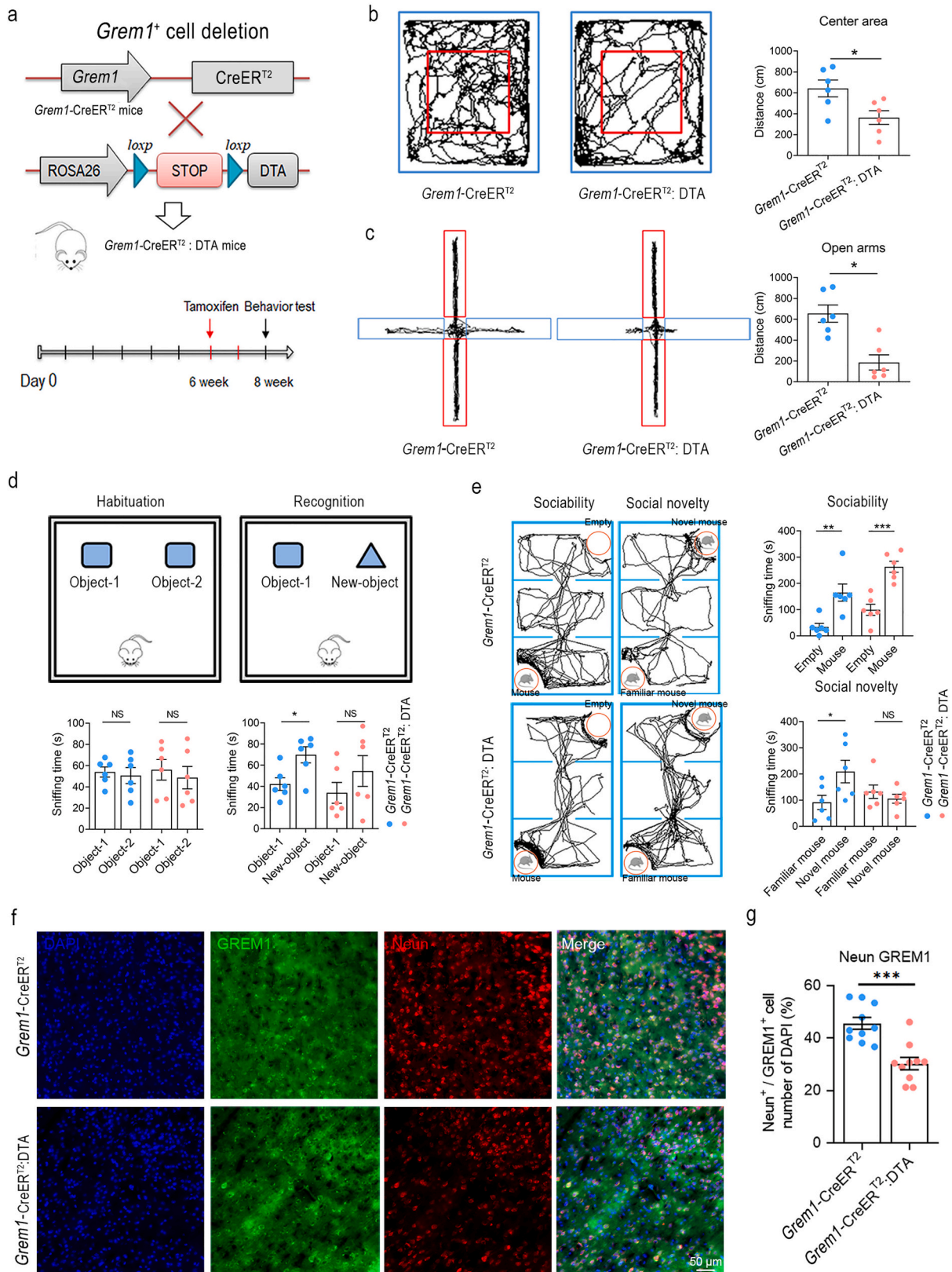
Fig. 6. Abnormal behavior and brain alternation of *Grem1*-CreER^{T2} : DTA mice at P56.
(a) Schematic diagram of the *Grem1*-CreER^{T2} : DTA mice reproductive strategies and timeline of tamoxifen gavage and behavioral tests in *Grem1*-CreER^{T2} and *Grem1*-CreER^{T2} : DTA mice. Behavior test in *Grem1*-CreER^{T2} and *Grem1*-CreER^{T2}: DTA mice, including (b) open field test, (c) elevated-plus-maze, (d) novel object recognition test and (e)Three-chamber social interaction test as well as the corresponding statistical graph. $n = 6$ mice / group. (f) brain alternation of *Grem1*-CreER^{T2} : DTA mice at P56 was observed by double immunofluorescence staining of Neun and GREM1, and (g) data analysis in the percentage of Neun$^+$ GREM1$^+$ cell to DAPI. ZEISS Axio Imager 2 microscope using a 40× / 0.95 NA objective. ($n = 10$ slices / group from 6 mice, Scale bars = 50 μm). Data are presented as means ± SEM. Statistical significance is determined by a two-tailed student *t*-test, ns, no significant. $p > 0.05$; *$p < 0.05$; **$p < 0.01$; ***$p < 0.001$; ****$p < 0.0001$.

the activation of FGFR1 and downstream MEK-ERK signaling (Cheng et al., 2022). GREM1 promotes proliferation and suppresses astrocyte differentiation of cancer stem cells in glioblastoma (Yan et al., 2014). Of note, it was reported that GREM1 may play paracrine/autocrine roles in tumor neovascularization (Mitola et al., 2010). Our results supported GREM1 exhibiting biological effects on target cells in an autocrine or a paracrine manner (Fig. S2a). Therefore, clearing GREM1-secreting cells may be an option for treating brain tumors, but one of the problems with this is that doing so perhaps damages normal cells. In addition, the function of GREM1-secreting cells, especially those with tdTomato-positive neurons, remains unclear. To assess the risks associated with this cell deletion strategy and to confirm the functional contribution of GREM1-secreting cells in normal brains, we deleted GREM1-secreting cells based on Cre recombination-mediated expression of the DTA. Consequently, we found that ablation of GREM1-secreting cells triggered anxiety-like behavior in mice and impaired their memory, including object and biological object memory. The histological analysis showed that the number of neurons significantly decreased in layers V and VI of the cerebral cortex in *Grem1*-CreER^{T2} : DTA$^+$ mice compared to mice in *Grem1*-CreER^{T2} group. Specifically, projections from layer V neurons in the cortical cortex to the spinal cord, cerebellum, striatum, and thalamus form a motor cortex circuit (Baker et al., 2018; Shipp, 2007), controlling movement preparation, guidance and the timely execution (Li et al., 2015). Emerging evidence suggests that layer VI neurons play a central role in modulating thalamic and cortical neurons during sensory processing (Wang et al., 2018), and pyramidal neurons exert high-level cognitive functions in the neocortex (Ichinose et al., 2021). Therefore, the observed decrease in layer V/VI neurons would give rise to impaired preparation for and coordination of movement in DTA$^+$ animals, explaining the motor balance defect in these animals in comparison with littermate controls. Similarly, our behavioral testing confirmed that tamoxifen-induced clearance of GREM1-secreting cells caused damage to neurons and microglia, implying a direct correlation between behavioral disorders and neuropathic alterations. However, it is worth noting that GREM1-secreting cells are not confined to the CNS, but abundantly expressed in the digestive system and bones. Recent research has indicated that GREM1 is primarily expressed in specific cells surrounding intestinal stem cells, including PDGFRA^{low} cells and CD81$^+$ cells within the mesenchymal layer (Kraiczy et al., 2023). The elimination of these GREM1-secreting cells might indirectly disrupt the growth and differentiation of intestinal stem cells, resulting in an imbalance in intestinal homeostasis. This imbalance may further influence behavioral abnormalities through the gut-brain axis. For example, previous study has shown that in mice with EphB6 deficiency-induced intestinal homeostatic imbalance, disruptions in gut microbiota balance led to deficiencies in vitamin B6 and dopamine neurons, impacting social behaviors in mice through the gut-brain axis (Li et al., 2020). Additionally, research employing *Grem1*-CreER^{T2} : R26-LSL-ZsGreen : R26-LSL-DTA mice with tamoxifen administration resulted in the clearance of GREM1-secreting cells, leading to impairments in skeletogenesis (Worthley et al., 2015), abnormalities of which are recognized as contributing factors to reduced motor ability. We considered that the abnormal behavioral phenotypes observed in *Grem1*-CreER^{T2} : DTA mice may primarily result from the elimination of GREM1-secreting cells in the CNS, but it is likely that the deletion of these cells in organs such as the digestive system and bone may also contribute to such behavioral deficits.

In conclusion, we found that GREM1 is ubiquitously expressed in the brain, especially in the gray matter such as Cx, Cb, and Th. Furthermore, we discovered that GREM1 is secreted mainly by excitatory neurons, and to a much lesser extent by microglia. Finally, by the tamoxifen-induced clearance of GREM1-secreting cells, we detected anxiety-like behavior and memory impairment in *Grem1*-CreER^{T2} : DTA mice. Of note, there was a significant decrease in neurons and microglia in the *Grem1*-CreER^{T2} : DTA mice brain, which in turn corroborates the synthesis of GREM1 by these two types of cells.

Credit authorship contribution statement

Peijia Yao: Conceptualization, Data curation, Methodology, Writing – original draft, Writing – review & editing. **Xueli Liu:** Methodology, Writing – review & editing, Data curation, Writing – original draft. **Qiang Miao:** Data curation, Methodology, Writing – original draft. **Changxue Li:** Data curation, Methodology, Writing – review & editing. **Huaixiang Zhou:** Investigation, Software, Visualization. **Huiliang Li:** Investigation, Software, Visualization. **Xinliang Mao:** Conceptualization, Supervision, Writing – review & editing. **Xiaoyi Fang:** Conceptualization, Funding acquisition, Supervision, Writing – review & editing. **Ningning Li:** Conceptualization, Funding acquisition, Supervision.

Declaration of Competing Interest

The authors declare no competing financial interests.

Data availability

Data will be made available on request.

Appendix A. Supplementary data

Supplementary data to this article can be found online at https://doi.org/10.1016/j.expneurol.2023.114649.

References

Antony, I., Narasimhan, M., Shen, R., Prakasam, R., Kaushik, K., Chapman, G., Kroll, K.L., 2023. Duplication versus deletion through the lens of 15q13.3: clinical and research implications of studying copy number variants associated with neuropsychiatric disorders in induced pluripotent stem cell-derived neurons. Stem Cell Rev. Rep. 19, 639–650.

Bachiller, D., Klingensmith, J., Kemp, C., Belo, J.A., Anderson, R.M., May, S.R., McMahon, J.A., McMahon, A.P., Harland, R.M., Rossant, J., Robertis, K.E.M.D., 2000. The Organizer Factors Chordin and Noggin are Required for Mouse Forebrain Development.

Baker, A., Kalmbach, B., Morishima, M., Kim, J., Juavinett, A., Li, N., Dembrow, N., 2018. Specialized subpopulations of deep-layer pyramidal neurons in the neocortex: bridging cellular properties to functional consequences. J. Neurosci. 38, 5441–5455.

Bal, Z., Kushioka, J., Kodama, J., Kaito, T., Yoshikawa, H., Korkusuz, P., Korkusuz, F., 2020. BMP and TGFbeta use and release in bone regeneration. Turk. J. Med. Sci. 50, 1707–1722.

Chang, J., Song, Z., Wei, S., Zhou, Y., Ju, J., Yao, P., Jiang, Y., Jin, H., Chi, X., Li, N., 2023. Expression mapping and functional analysis of orphan G-protein-coupled receptor GPR158 in the adult mouse brain using a GPR158 transgenic mouse. Biomolecules 13.

Cheng, C., Wang, J., Xu, P., Zhang, K., Xin, Z., Zhao, H., Ji, Z., Zhang, M., Wang, D., He, Y., Jing, N., Fan, L., Liu, K., Li, F., Liu, C., Gong, Y., Cui, S., Sun, Z., Sun, D.,

Yao, X., Li, H., Zhang, J., Zhang, P., Dong, B., Xue, W., Qian, X., Gao, W.Q., Zhu, H. H., 2022. Gremlin1 is a therapeutically targetable FGFR1 ligand that regulates lineage plasticity and castration resistance in prostate cancer. Nat. Cancer 3, 565–580.

Church, R.H., Krishnakumar, A., Urbanek, A., Geschwindner, S., Meneely, J., Bianchi, A., Basta, B., Monaghan, S., Elliot, C., Stromstedt, M., Ferguson, N., Martin, F., Brazil, D. P., 2015. Gremlin1 preferentially binds to bone morphogenetic protein-2 (BMP-2) and BMP-4 over BMP-7. Biochem. J. 466, 55–68.

Claesson-Welsh, L., 2010. Gremlin: vexing VEGF receptor agonist. Blood 116, 3386–3387.

Correns, A., Zimmermann, L.A., Baldock, C., Sengle, G., 2021. BMP antagonists in tissue development and disease. Matrix Biol. Plus 11, 100071.

David, C.J., Massague, J., 2018. Contextual determinants of TGFbeta action in development, immunity and cancer. Nat. Rev. Mol. Cell Biol. 19, 419–435.

Ding, P., Chen, W., Yan, X., Zhang, J., Li, C., Zhang, G., Wang, Y., Li, Y., 2022. BMPER alleviates ischemic brain injury by protecting neurons and inhibiting neuroinflammation via Smad3-Akt-Nrf2 pathway. CNS Neurosci. Ther. 28, 593–607.

Donnelly, L.E., H., G., L., H., M., E., T.D., D., G, 2001. The 'cleavage' activities of foot-and-mouth disease virus 2A site-directed mutants and naturally occurring '2A-like' sequences. J. Gen. Virol. 82 (Pt 85), 1027–1041.

Fan, Q., Zhou, J., Wang, Y., Xi, T., Ma, H., Wang, Z., Xiao, W., Liu, Q., 2020. Chip-based serum proteomics approach to reveal the potential protein markers in the sub-acute stroke patients receiving the treatment of Ginkgo Diterpene lactone Meglumine injection. J. Ethnopharmacol. 260, 112964.

Furuta, Y., Piston, D.W., Hogan, B.L.M., 1997. Bone Morphogenetic Proteins (BMPs) as Regulators of Dorsal Forebrain Development. BMPs and Dorsal Forebrain Development.

Gazzerro, E., Smerdel-Ramoya, A., Zanotti, S., Stadmeyer, L., Durant, D., Economides, A. N., Canalis, E., 2007. Conditional deletion of gremlin causes a transient increase in bone formation and bone mass. J. Biol. Chem. 282, 31549–31557.

Hart, C.G., Karimi-Abdolrezaee, S., 2020. Bone morphogenetic proteins: new insights into their roles and mechanisms in CNS development, pathology and repair. Exp. Neurol. 334, 113455.

Ichinose, M., Suzuki, N., Wang, T., Kobayashi, H., Vrbanac, L., Ng, J.Q., Wright, J.A., Lannagan, T.R.M., Gieniec, K.A., Lewis, M., Ando, R., Enomoto, A., Koblar, S., Thomas, P., Worthley, D.L., Woods, S.L., 2021. The BMP antagonist gremlin 1 contributes to the development of cortical excitatory neurons, motor balance and fear responses. Development 148.

Kraiczy, J., McCarthy, N., Malagola, E., Tie, G., Madha, S., Boffelli, D., Wagner, D.E., Wang, T.C., Shivdasani, R.A., 2023. Graded BMP signaling within intestinal crypt architecture directs self-organization of the Wnt-secreting stem cell niche. Cell Stem Cell 30, 433–449 e438.

Li, N., Chen, T.W., Guo, Z.V., Gerfen, C.R., Svoboda, K., 2015. A motor cortex circuit for motor planning and movement. Nature 519, 51–56.

Li, Y., Luo, Z.Y., Hu, Y.Y., Bi, Y.W., Yang, J.M., Zou, W.J., Song, Y.L., Li, S., Shen, T., Li, S. J., Huang, L., Zhou, A.J., Gao, T.M., Li, J.M., 2020. The gut microbiota regulates autism-like behavior by mediating vitamin B(6) homeostasis in EphB6-deficient mice. Microbiome 8, 120.

Maiolo, D., Mitola, S., Leali, D., Oliviero, G., Ravelli, C., Bugatti, A., Depero, L.E., Presta, M., Bergese, P., 2012. Role of nanomechanics in canonical and noncanonical pro-angiogenic ligand/VEGF receptor-2 activation. J. Am. Chem. Soc. 134, 14573–14579.

Manzari-Tavakoli, A., Babajani, A., Farjoo, M.H., Hajinasrollah, M., Bahrami, S., Niknejad, H., 2022. The cross-talks among bone morphogenetic protein (BMP) signaling and other prominent pathways involved in neural differentiation. Front. Mol. Neurosci. 15, 827275.

Marquez-Exposito, L., C.-N.E, Rodrigues-Diez, R., et al., 2020. Molecular regulation of notch signaling by Gremlin. Adv. Exp. Med. Biol. 81–94.

Mitola, S., Ravelli, C., Moroni, E., Salvi, V., Leali, D., Ballmer-Hofer, K., Zammataro, L., Presta, M., 2010. Gremlin is a novel agonist of the major proangiogenic receptor VEGFR2. Blood 116, 3677–3680.

Ouellette, J., Toussay, X., Comin, C.H., Costa, L.D.F., Ho, M., Lacalle-Aurioles, M., Freitas-Andrade, M., Liu, Q.Y., Leclerc, S., Pan, Y., Liu, Z., Thibodeau, J.F., Yin, M., Carrier, M., Morse, C.J., Dyken, P.V., Bergin, C.J., Baillet, S., Kennedy, C.R., Tremblay, M.E., Benoit, Y.D., Stanford, W.L., Burger, D., Stewart, D.J., Lacoste, B., 2020. Vascular contributions to 16p11.2 deletion autism syndrome modeled in mice. Nat. Neurosci. 23, 1090–1101.

Petersen, M.A., Tognatta, R., Meyer-Franke, A., Bushong, E.A., Mendiola, A.S., Yan, Z., Muthusamy, A., Merlini, M., Meza-Acevedo, R., Cabriga, B., Zhou, Y., Thomas, R., Ryu, J.K., Lassmann, H., Ellisman, M.H., Akassoglou, K., 2021. BMP receptor blockade overcomes extrinsic inhibition of remyelination and restores neurovascular homeostasis. Brain 144, 2291–2301.

Phani, S., Jablonski, M., Pelta-Heller, J., Cai, J., Iacovitti, L., 2013. Gremlin is a novel VTA derived neuroprotective factor for dopamine neurons. Brain Res. 1500, 88–98.

Pous, L., Deshpande, S.S., Nath, S., Mezey, S., Malik, S.C., Schildge, S., Bohrer, C., Topp, K., Pfeifer, D., Fernandez-Klett, F., Doostkam, S., Galanakis, D.K., Taylor, V., Akassoglou, K., Schachtrup, C., 2020. Fibrinogen induces neural stem cell differentiation into astrocytes in the subventricular zone via BMP signaling. Nat. Commun. 11, 630.

Rowan, S.C., J.H, Mthunzi, L., Piouceau, L., Cornwell, J., Doody, R., Frohlich, S., Callanan, J.J., McLoughlin, P., 2020. Gremlin 1 depletion in vivo causes severe enteropathy and bone marrow failure. J. Pathol. 251, 117–122.

Setoguchi, T., Nakashima, K., Takizawa, T., Yanagisawa, M., Ochiai, W., Okabe, M., Yone, K., Komiya, S., Taga, T., 2004. Treatment of spinal cord injury by transplantation of fetal neural precursor cells engineered to express BMP inhibitor. Exp. Neurol. 189, 33–44.

Shipp, S., 2007. Structure and function of the cerebral cortex. Curr. Biol. 17, R443–R449.

Söderström, S., Bengtsson, H., Ebendal, T., 1996. Expression of Serine/Threonine Kinase Receptors Including the Bone Morphogenetic Factor Type II Receptor in the Developing and Adult Rat Brain.

Sun, Y., Yan, K., Wang, Y., Xu, C., Wang, D., Zhou, W., Guo, S., Han, Y., Tang, L., Shao, Y., Shan, S., Zhang, Q.C., Tang, Y., Zhang, L., Xi, Q., 2022. Context-dependent tumor-suppressive BMP signaling in diffuse intrinsic pontine glioma regulates stemness through epigenetic regulation of CXXC5. Nat. Cancer 3, 1105–1122.

Topol, L.Z., M.W, Koochekpour, S., Blair, D.G., 2000. DRM/GREMLIN (CKTSF1B1) maps to human chromosome 15 and is highly expressed in adult and fetal brain. Cytogenet. Cell Genet. 79–84.

Wang, W., Andolina, I.M., Lu, Y., Jones, H.E., Sillito, A.M., 2018. Focal gain control of thalamic visual receptive fields by layer 6 corticothalamic feedback. Cereb. Cortex 28, 267–280.

Worthley, D.L., Churchill, M., Compton, J.T., Tailor, Y., Rao, M., Si, Y., Levin, D., Schwartz, M.G., Uygur, A., Hayakawa, Y., Gross, S., Renz, B.W., Setlik, W., Martinez, A.N., Chen, X., Nizami, S., Lee, H.G., Kang, H.P., Caldwell, J.M., Asfaha, S., Westphalen, C.B., Graham, T., Jin, G., Nagar, K., Wang, H., Kheirbek, M.A., Kolhe, A., Carpenter, J., Glaire, M., Nair, A., Renders, S., Manieri, N., Muthupalani, S., Fox, J.G., Reichert, M., Giraud, A.S., Schwabe, R.F., Pradere, J.P., Walton, K., Prakash, A., Gumucio, D., Rustgi, A.K., Stappenbeck, T.S., Friedman, R. A., Gershon, M.D., Sims, P., Grikscheit, T., Lee, F.Y., Karsenty, G., Mukherjee, S., Wang, T.C., 2015. Gremlin 1 identifies a skeletal stem cell with bone, cartilage, and reticular stromal potential. Cell 160, 269–284.

Yan, K., Wu, Q., Yan, D.H., Lee, C.H., Rahim, N., Tritschler, I., DeVecchio, J., Kalady, M. F., Hjelmeland, A.B., Rich, J.N., 2014. Glioma cancer stem cells secrete Gremlin1 to promote their maintenance within the tumor hierarchy. Genes Dev. 28, 1085–1100.

Yuzwa, S.A., Borrett, M.J., Innes, B.T., Voronova, A., Ketela, T., Kaplan, D.R., Bader, G. D., Miller, F.D., 2017. Developmental emergence of adult neural stem cells as revealed by single-cell transcriptional profiling. Cell Rep. 21, 3970–3986.